Natural lakes are a minor global source of N2O to the atmosphere

R. Lauerwald, P. Regnier, V Figueiredo, Alex Enrich Prast, David Bastviken, B. Lehner, T. Maavara and P. Raymond

Tweet

LINKÖPING UNIVERSITY

Natural lakes are a minor global source of N₂O to the atmosphere

R. Lauerwald[1], P. Regnier[1], V. Figueiredo[2], A. Enrich-Prast[2,3], D. Bastviken[3], B. Lehner[4], T. Maavara[5], P. Raymond[6]

[1]Biogeochemistry and Earth System Modelling, Department of Geoscience, Environment and Society, Université Libre de Bruxelles, Bruxelles, 1050 Brussels, Belgium

[2]Pos Graduation in Biotechnology, University Federal of Rio de Janeiro, 21941-590 Rio de Janeiro, Brazil

[3]Department of Thematic Studies - Environmental Change Linköping University, 581 83 Linköping, Sweden

[4]Department of Geography, McGill University, Burnside Hall, 805 Sherbrooke Street West, Montreal, QC H3A 0B9, Canada

[5]Earth and Environmental Sciences Area, Lawrence Berkeley National Laboratory, 1 Cyclotron Rd., Berkeley, CA, 94720, USA

[6]Yale School of Forestry and Environmental Studies, New Haven, Connecticut 06511, USA

Corresponding author: Ronny Lauerwald (ronny.lauerwald@ulb.ac.be)

Key Points:

- Global N₂O emission from natural lakes and reservoirs estimated at 4.5 ± 2.9 Gmol N yr⁻¹

- Natural lakes emit less N₂O than reservoirs

- North America and Europe contribute nearly half of global N₂O emission from natural lakes and reservoirs

Abstract

Natural lakes and reservoirs are important, yet not well constrained sources of greenhouse gasses to the atmosphere. In particular for N_2O emissions, a huge variability is observed in the few, observation-driven flux estimates that have been published so far. Recently, a process-based, spatially explicit model has been used to estimate global N_2O emissions from more than 6,000 reservoirs based on nitrogen (N) and phosphorous inflows and water residence time. Here, we extend the model to a dataset of 1.4 million standing water bodies comprising natural lakes and reservoirs. For validation, we normalized the simulated N_2O emissions by the surface area of each water body and compared them against regional averages of N_2O emission rates taken from the literature or estimated based on observed N_2O concentrations. We estimate that natural lakes and reservoirs together emit 4.5 ± 2.9 Gmol N_2O-N yr^{-1} globally. Our global scale estimate falls in the far lower end of existing, observation-driven estimates. Natural lakes contribute only about half of this flux, although they contribute 91% of the total surface area of standing water bodies. Hence, the mean N_2O emission rates per surface area are substantially lower for natural lakes than for reservoirs with 0.8 ± 0.5 mmol N m^{-2}yr^{-1} vs. 9.6 ± 6.0 mmol N m^{-2}yr^{-1}, respectively. This finding can be explained by on average lower external N inputs to natural lakes. We conclude that upscaling based estimates, which do not distinguish natural lakes from reservoirs, are prone to important biases.

1 Introduction

Inland waters are important sources of greenhouse gasses to the atmosphere. However, global scale estimates are afflicted by large uncertainties, in particular for nitrous oxide (N_2O), which is the third most important long-lived greenhouse gas. In its fifth assessment, the IPCC reports existing estimates of total N_2O emissions from continental waters with a range of 7.1 to 207.1 Gmol N yr^{-1}, representing a warming potential of 0.1-2.7 Pg CO_2-eq. yr^{-1} on a 100 year time horizon [*Ciais et al., 2013*]. This estimate for continental waters comprises only rivers, estuaries and the coastal zone and excludes standing water bodies (SWB) defined here as the sum of natural lakes and reservoirs (artificial lakes created by damming).

While global estimates of N_2O emissions from running waters have been presented in a number of studies [*Beaulieu et al., 2011*; *Hu et al., 2016*; *Kroeze et al., 2005*, *2010*; *Seitzinger et al., 2000*], the first global estimate for SWBs was published in 2015 by *Soued et al.*. They estimated a global N_2O emission of 45.0 ± 21.1 Gmol N yr^{-1}. Three years later, *DelSontro et al.* [*2018*] reassessed these emissions using simple upscaling and different estimates of global SWB surface area, as well as an empirical model relating N_2O emission rates to lake productivity and lake size, obtaining values ranging from 11.3 Gmol N yr^{-1} to 27.1 Gmol N yr^{-1}. While the studies by *Soued et al.* and *DelSontro* et al. did not distinguish natural lakes from reservoirs, *Deemer et al.* [*2016*]

estimated a global emission of 2.4 Gmol N_2O-N yr^{-1} from reservoirs only. The large uncertainties in these estimates, however, do not allow to assess with confidence the relative contributions of reservoirs and natural lakes to the overall N_2O emissions from SWB. For this, a consistent methodological framework that distinguishes both types of water bodies is needed.

The studies by *Soued et al.* [2015], *Deemer et al.* [2016], and *DelSontro et al.* [2018] used an upscaling technique which consists in multiplying an averaged, observation based N_2O flux rate by an estimate of the total water surface area. The low number and uneven distribution of SWB N_2O data explain the large uncertainty in flux estimates, and may also cause a bias in the upscaling. *Soued et al.* [2015] based their estimate on their own observations in Quebec and 157 literature values, of which 137 (88%) were from the temperate zone. *Deemer et al.* [2016] up-scaled their global value from observed fluxes of only 58 reservoirs. *DelSontro et al.* [2018] have used the largest amount of literature data so far, comprising in total 309 observed N_2O emission rates. In addition, uncertainties still exist with regard to the total surface area, number and size distribution of SWBs at global scale [*Fluet-Chouinard et al., 2016*], and the use of different estimates and data sets leads to very different upscaled results as demonstrated by *DelSontro et al.* [2018]. Moreover, the three global studies so far give lumped estimates of SWB N_2O emissions without exploring the global scale spatial patterns. Due to the uneven global coverage of observed N_2O emission rates, it is not possible to explore the global scale spatial pattern of N_2O emissions from SWBs based on empirical upscaling. Global estimates of riverine N_2O emission [*Beaulieu et al., 2011*; *Hu et al., 2016*; *Kroeze et al., 2005*], on the contrary, rely on empirically estimated emission factors linearly relating N_2O emission rates to riverine N loads, which were then applied to global scale assessments of riverine N loads. Existing, spatially explicit representations of riverine N loads [e.g. *Mayorga et al., 2010*] permitted for similarly spatially explicit estimates of riverine N_2O emission estimates [e.g. *Hu et al.*, 2016].

Recently, *Maavara et al.* [2019] developed a process-oriented model to consistently estimate N_2O emissions from a broad range of inland waters, including reservoirs. Based on a spatially explicit representation of the river-reservoir network and point and non-point sources of nitrogen (N) and phosphorous (P), this model made it possible to explore and quantify the global scale spatial patterns in riverine and reservoir N_2O emissions in a consistent manner. In this study, we apply the approach of *Maavara et al.* [2019] to a global data set of 1.4 million SWBs which

are classified into natural lakes and reservoirs [*Messager et al., 2016*]. Model results for N_2O emissions from SWBs are evaluated against regional, observation-driven estimates.

The main objectives of our study are to predict and analyze the global scale spatial patterns in N_2O emissions from all standing waters and to quantify the contribution of natural lakes vs. reservoirs to the global N_2O emission flux. We hypothesize that these contributions largely scale with their contribution to the overall water surface area. We thus expect global N_2O emissions from SWBs to be dominated by the contributions from natural lakes as they contribute 91% of the global SWB surface area [*Messager et al., 2016*]. Further, we hypothesize that global scale spatial patterns of these emissions follow largely the distribution of SWB surface areas, and are therefore different from the spatial patterns of riverine N_2O emissions. This would be consistent with what was found for riverine vs. SWB emissions of CO_2 [*Raymond et al., 2013*].

2 Materials and Methods

In this study, we make use of a methodological framework recently established to estimate N_2O emissions from inland waters [*Maavara et al.*, 2019]. The model structure was kept simple to be applicable to a broad range of inland water types; and indeed the global scale results from *Maavara et al.* [2019] using this model are comparable to the results of recent, measurement-based upscaling methods used for reservoirs [*Deemer et al., 2016*] and rivers [*Hu et al., 2016*]. To date this methodology has been applied to rivers, reservoirs and estuaries [*Maavara et al.*, 2019]. Here we apply it to a data set of 1.4 million SWBs, which include both natural lakes and reservoirs [*Messager et al.*, 2016]. In the following, we provide an overview about the model construction (section 2.1), before we describe the preparation of input data sets and the global scale application of the model (section 2.2) and the evaluation of model outputs against observation-driven estimates based on literature data (section 2.3).

2.1 N-model

For their global estimate, *Maavara et al.* [2019] used a set of simple equations that predict the N budget and N_2O emission of each inland water body based on inputs of total N (TN_{in}) and total P (TP_{in}) from the watershed and the water residence time τ_r. It was, however, impossible to train these equations directly on observed data due to the limited amount of empirical work available to constrain these specific relations. To overcome that limitation, *Maavara et al.* [2019] developed a generalized, mechanistic mass balance model which represents all important

biogeochemical processes involved in aquatic N cycling, and which is valid for a broad range of inland water types including rivers, reservoirs and estuaries. The major biogeochemical processes represented by the model include primary production, nitrification, denitrification, mineralization, solubilization, N fixation and burial of N in sediments as well as N_2O production and N_2O emission (see Figure S1). That model itself could not directly be applied for a spatially explicit estimation of N_2O emissions from inland waters at the global scale due to the lack of geodata representing all necessary drivers. Instead, the model was fed with hypothetical but realistic combinations of parameters defining inland water properties (water body volume, discharge, surface area, temperature, and elevation), parameters defining quantity and quality of nutrient inputs, and parameters defining the kinetics of all biogeochemical processes involved. For all these parameters, *Maavara et al.* [2019] defined probability density functions (PDFs) approximating the global statistical distribution of those parameters as derived from literature values and databases. Then, the model was run in a Monte Carlo simulation with 8,000 iterations randomly choosing parameter values from these PDFs and generating a database of annual N cycling, N_2O production and N_2O emission rates in/from 8,000 hypothetical water bodies spanning the entire parameter space of physical characteristics. This database was then used to fit the simpler equations relating inland water N and N_2O budgets to TN_{in}, TP_{in}, and τ_r, which were then used for the global upscaling. A similar strategy was previously applied to quantify global-scale silica, phosphorous and organic carbon cycling in reservoirs [*Maavara et al.*, 2014, 2015, 2017]. In the following, we briefly summarize the fitted equations used for upscaling the nitrification, denitrification, N fixation and burial fluxes defining the N and P budget of each water body. For more details on the mechanistic model used to produce that database, we would like to refer to the original publication by *Maavara et al.* [2019]. Next, we give more detailed explanations on the assumptions and equations used to simulate N_2O production and emission, which were slightly adapted here and which are of central interest for our study.

The nitrification (*Nitrif*) and denitrification (*Denit*) rates as well as the burial flux of N (*TN_burial*) were fitted to equations using as predictors the total input of N, i.e. the sum of TN_{in} and the nitrogen fixation flux (*Fix*), and the water residence time τ_r, assuming that the dependence follows an error function ("erf", eqs. 1 to 3), i.e. a sigmoid-shaped, monotonically increasing function that asymptotically approaches a maximum value for high τ_r.. The mean and median τ_r of the 1.4 million SWBs in the HydroLAKES dataset used here are 4.9 years and 1.2 years,

respectively, with 1% of the water bodies having a τ_r of 50 years and longer. If the molar ratio $TN_{in}:TP_{in}$ is lower than 30, *Fix* is calculated according to equations 4 and 5 while for higher $TN_{in}:TP_{in}$ ratios, *Fix* is assumed to be zero. First, the fraction of *Fix* on the total N input to the water body (N_{fix}) is estimated from $TN_{in}:TP_{in}$ and τ_r (eq. 4). Then, *Fix* is calculated from TN_{in} and N_{fix} (eq. 5). The outflow of N is then calculated by subtracting the losses due to *Denit* and TN_{burial} from the total N inputs (TN_{in} + *Fix*). Phosphorus is lost from the water column only by burial in sediments (TP_{burial}) which is as well estimated from τ_r [*Taylor Maavara et al., 2015*] (eq. 6).

$$Nitrif = (TN_{in} + Fix)[0.5144 \times \mathrm{erf}(0.3692\,\tau_r)] \qquad (1)$$

$$Denit = (TN_{in} + Fix)[0.3833 \times \mathrm{erf}(0.4723\,\tau_r)] \qquad (2)$$

$$TN_{burial} = (TN_{in} + Fix)[0.51 \times \mathrm{erf}(0.4723\,\tau_r)] \qquad (3)$$

$$N_{fix}\,(\%) = \frac{37.2}{(1+\exp(0.5\times TNin:TPin-6.877))} \times \mathrm{erf}(\tfrac{\tau_r-0.028}{0.04}) \qquad (4)$$

$$Fix = \frac{TN_{in}\times N_{fix}}{(1-N_{fix})} \qquad (5)$$

$$TP_{burial} = TP_{in}\left[1 - \frac{1}{1+0.754\cdot\tau_r}\right] \qquad (6)$$

In the above equations, τ_r is given in years, N_{fix} is expressed in % and all other variables are in moles of N or P per year. Numerical values in eqns. 1-3 and 6 were obtained from fitting the mechanistic model outputs.

As reviewed in *Maavara et al.* [2019], N_2O production and/or emissions have in earlier studies been estimated from nitrification/denitrification rates or from N loads based on empirically derived emission factors (*EFs*). The wide range of published *EFs* is one of the main reasons for the wide range of existing N_2O emission estimates. When scaled to process rates, the *EFs* correspond to the production of a relatively small fraction of N in the form of N_2O during incomplete nitrification and denitrification. When these processes are complete, ammonium is entirely oxidized to nitrate (nitrification) and nitrate is entirely reduced to dinitrogen gas (denitrification). Following Maavara et al. (2019), the *EFs* used in our mechanistic model allows to estimate the production of N_2O (N_2O_{prod}) from simulated *Denit* and *Nitrif* rates (eq. 7). Further in agreement with that study, we adopted an *EF* of 0.9% (for both denitrification and nitrification) as best estimate, which was derived as arithmetic mean of 40 literature values reviewed by *Beaulieu et al.* [*2011*]. For a lower-bound estimate of N_2O_{prod}, we chose an alternative *EF*=0.3%

representing the arithmetic mean of the 20 lower values reported by Beaulieu et al. Similarly, we derived an alternative $EF=1.5\%$ as the arithmetic mean of the 20 higher values referenced therein to calculate an upper-bound estimate of N_2O_{prod}.

$$N_2O_{prod,DS1} = N_2O_{em,DS1} = EF \times (Nitrif + Denit) \qquad (7)$$

In order to estimate the N_2O emission flux (N_2O_{em}) we applied the two "default simulation" set-ups DS1 and DS2 used in *Maavara et al.* [2019]. DS1 represents a simplified approach that assumes N_2O_{em} to equal N_2O_{prod}, thus using eq. 7 for the global upscaling of N_2O_{em}. For DS2, in contrast, it was taken into account that in the process of denitrification, the initially produced N_2O can further be reduced to N_2 if it is not evading sufficiently rapidly from the water column. Inclusion of this loss term required the explicit representation of the N_2O pool in the mechanistic model (Figure S1). To account for the progressive consumption of N_2O produced via denitrification in water bodies with long τ_r, the EF (0.9%, 0.3%, or 1.5%, see above) was modulated by the inverse function of the term in square brackets in eq. 2 in such a way that N_2O production now reads:

$$N_2O_{prod,DS2} = EF \times (Nitrif + Denit \times (0.4372\, erfc(0.4697\, \tau_r))) \quad (8)$$

Note that for nitrification, we are considering that N_2O is not consumed, and the *EF* in DS2 is the same as in DS1. N_2O emission in DS2 was then calculated assuming that only the fraction of N_2O that is super-saturated with respect to the equilibrium atmospheric N_2O concentration is emitted. Since N_2O production and emission differ in DS2, a new Monte Carlo simulation was performed for this scenario, and from the output, a single equation for the total (nitrification+denitrification) N_2O emissions was fitted (eq. 9). Note that this empirical equation relates the N_2O emissions directly to TN_{in} and τ_r, and thus represents denitrification and nitrification as N_2O sources in an implicit manner.

$$N_2O_{em,DS2} = TN_{in}[a \times erf(b \times \tau_r)] \qquad (9)$$

with *a*=2.28e-3, 0.79e-3, or 3.79e-3, and *b*=1.63, 1.96, or 1.62 for an *EF*=0.9%, 0.3%, or 1.5%, respectively.

Figure 1 illustrates the difference between DS1 and DS2 in simulated N_2O_{em} relative to N inputs as function of τ_r and the *EF* chosen. As upper-bound (EF=1.5%) and lower bound (EF=0.3%) estimates deviate from the best estimate (EF=0.9%) in a close to symmetric way, we report our bounded estimates as best estimate ± average difference from the bounds. Note that up to a τ_r of 7 months, both scenarios give relatively similar emission rates. For higher τ_r, DS2 gives consistently lower N_2O_{em} estimates, and the maximum ratio N_2O_{em} to N inputs is reached already after about 1 year, while under DS1 that ratio keeps increasing up to a τ_r of about 5 years.
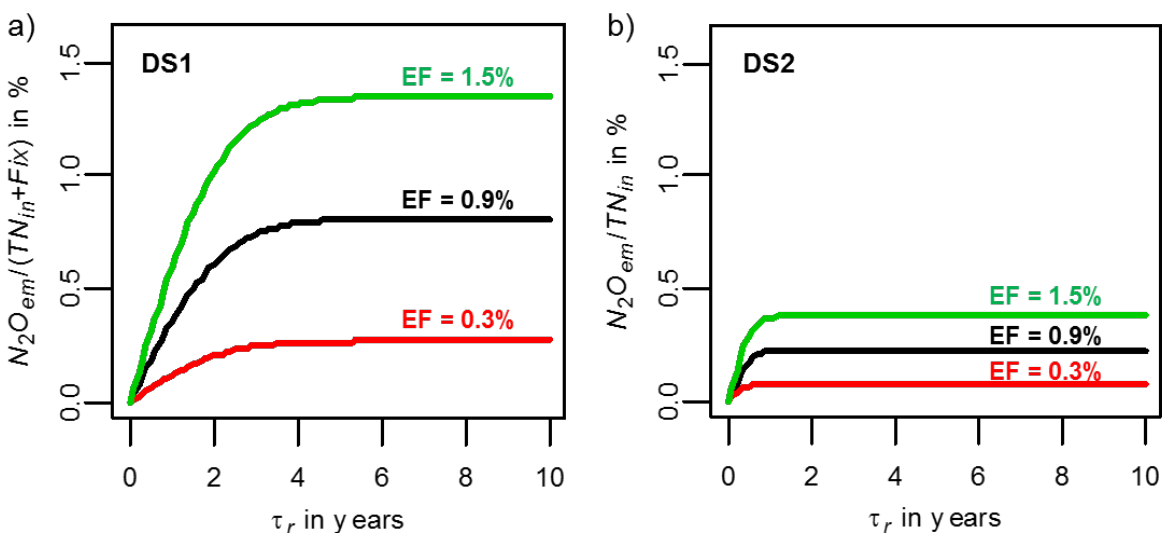

Figure 1: Simulated N$_2$O emissions (N_2O_{em}) as function of water residence time τ_r following scenario DS1 (eq. 7, panel a) and DS2 (eq. 9 panel b). For each scenario, we plotted the function using the EFs of 0.9%, 0.3% and 1.5% (see text). Simulated N_2O_{em} scale linearly with N input from upstream (TN_{in}, DS2) or the sum of TN_{in} and N fixation (*Fix*) (DS1). In this graph, we normalized N_2O_{em} accordingly.

2.2 Preparation of standing water body dataset

The global HydroLAKES database [*Messager et al., 2016*] contains information on 1.4 million SWBs with a minimum surface area of 0.1 km^2, including their surface polygons and associated area, their upstream watershed area, and estimates of water volume and water residence time τ_r. HydroLAKES distinguishes three different types of SWBs: 1) natural lakes without dam constructions, 2) reservoirs and 3) natural lakes hydrologically regulated by dam constructions. The latter two types of water bodies cover only 6,796 cases and were taken from the Global

Reservoir and Dam (GRanD) database [*Lehner et al., 2011*], which was used in the study of *Maavara et al.* [2019]. For our study, we use the classification of SWBs as defined in HydroLAKES, but, as long as not indicated otherwise, combine classes 1) and 3) as "natural lakes" (i.e. natural origin). We chose the HydroLAKES database over remote sensing derived maps in raster format [e.g. *Verpoorter et al.*, 2014] or statistical approaches [e.g. *Downing et al.*, 2012] as it uniquely provides individual SWB surface polygons that can be topologically connected within the river network based on their outlet coordinates which are associated with the drainage network of the global HydroSHEDS database at 15 arc-second (~500 m) spatial resolution [*Lehner et al., 2008*].

In order to estimate the TN_{in} and TP_{in} loads to each SWB, we combined the information of HydroLAKES with a spatially explicit representation of TN and TP mobilization from the watershed into the river network [after *Bouwman et al., 2009; Van Drecht et al., 2009; Mayorga et al.*, 2010; see *Maavara et al*, 2019 for details]. In short, we redistributed the yields of dissolved inorganic and organic, as well as particulate, N and P from point and non-point terrestrial sources, as they are represented in the GlobalNEWS v2 model, over a 0.5° raster. Then, we overlaid that raster with the HydroLAKES database. To find the N and P terrestrial contributions to each natural lake or reservoir, we multiplied the TN and TP yields by the direct upstream watershed area (net-watershed), i.e. excluding those areas that are intercepted by upstream lying SWBs. Furthermore, we added the TN and TP outflows of upstream SWBs as TN and TP inputs to downstream lying SWBs, following the topologic information provided by the HydroSHEDS drainage network. Following the methodology described in *Maavara et al.* [2019], we used the watershed area of, and the distance between SWBs to estimate the average riverine travel time of N and P from the terrestrial sources to the SWB and from the outlet of one SWB to the next downstream lying SWB, respectively. This travel time is used as τ_r to estimate gains of N through fixation (eqs. 4 & 5) and losses of N through denitrification (eq. 2) during riverine transport. Losses of N and P due to burial are assumed to be zero during riverine transport. In order to apply this model to the global dataset, we calculated the N and P budgets of SWBs in sequence from upstream to downstream so that outflows from SWBs can easily be cascaded to the next downstream lying SWB. Further, we estimated the TN concentration in each SWB by dividing the simulated TN outflow by the discharge reported in HydroLAKES, assuming concentrations in the outflow to equal average concentration in the water column.

2.3 Validation against observation-based flux estimates.

We compared our simulation results of N_2O emissions against regional estimates based on literature values of N_2O emission rates or N_2O concentrations. In case only N_2O concentrations were reported, we calculated emission rates based on an a gas exchange velocity k_{600} estimated from water body size [*Read et al., 2012*], water temperature and an assumed atmospheric partial pressure of N_2O ($p_{N_2O_{atm}}$) of 0.32 µatm for studies after 2000, and 0.31 µatm for studies before 2000, respectively (see below) (eqs. 10,11). *Read et al.* [2012] report average k_{600} values for four SWB size classes. The k_{600} values are increasing with water surface area, which is reflecting the stronger wind shear effect over a larger fetch [*Read et al., 2012*]. Water temperature was used to calculate the solubility constant K_{N_2O} after *Weiss and Price* [*1980*] (eq. 11) and the Schmidt number (*Sc*) for N_2O after *Wanninkhof* [*1992*], assuming salinity to be zero (eq. 12). In case water temperature was not reported, we used the empirical equation from *Lauerwald et al.* [*2015*] (eq. 13) to estimate the mean annual water temperature from mean annual air temperature at the location of the SWB which was in turn derived from the WorldClim2 database at 1 km spatial resolution [*Fick & Hijmans, 2017*].

$$N_2O_{em,obs} = \left(c_{N_2O_{aq}} - p_{N_2O_{atm}} \cdot K_{N_2O}\right) \cdot k_{600} \cdot \left(\frac{Sc}{600}\right)^{-0.5} \qquad (10)$$

$$\ln\left(K_{N_2O}\right) = -62.7062 + 97.3066 * \frac{100}{T_{water}} + 24.1406 * \ln\left(\frac{T_{water}}{100}\right) \qquad (11)$$

With:

$N_2O_{em,obs}$	Observation based estimate of emission rate of N_2O in mmol N m^{-2} day-1
$c_{N_2O_{aq}}$	Concentration of N_2O-N in the epilimnion of the SWB in µM
$p_{N_2O_{atm}}$	Partial pressure of N_2O in the atmosphere in µatm
K_{N_2O}	Solubility constant for N_2O-N in M atm^{-1}
T_{water}	Water temperature, here in K

$$Sc = 2056 - 137.11 \cdot T_{water} + 4.317 \cdot T_{water}^2 - 0.0543 \cdot T_{water}^3 \qquad (12)$$

$$T_{water} = 3.941 + 0.818 * T_{air} \qquad (13)$$

With:

T_{water}	Water temperature, here in °C
T_{air}	Air temperature, here in °C

We chose to compare simulated N_2O emissions vs. observation based estimates per regions, i.e. for a group of SWBs, rather than performing an evaluation of simulation results for individual SWBs for three main reasons:

1) The HydroLAKES database used for our model gives names only for the largest SWBs, and it is thus difficult to identify individual medium sized or small SWBs described in the literature.

2) Our global scale modelling approach is too coarse to give reliable estimates for individual SWBs, in particular as TN and TP mobilization from the watershed to individual SWBs are derived from global scale, empirical models at 0.5 degree resolution (see section 2.2)

3) The number of observations per SWB is in most cases rather low, and the uncertainties on whether these observations are representative of average annual emission fluxes are high and unconstrained considering the high temporal and small-scale spatial variations within each water body.

1   **Table 1.** Sources and methodologies used for regionalized, observation based N_2O emission rates used for model evaluation.

Region	Source for observation based flux estimate	Selection of simulation results as reference
Finland	observed N_2O emission rates from 8 natural lakes [*Huttunen et al.* 2002, 2003a, 2003b, 2004]	results from all natural lakes in Finland (N=7,891)
Switzerland	calculated from reported N_2O concentrations water surface area from 14 SWBs [*Mengis et al.*, 1997] and average T_{water} estimated from T_{air}	results from the same SWBs identified in HydroLAKES by name and location (N=14)
Tianjin region (China)	Observed N_2O emission rates from 10 natural lakes [*Liu et al.*, 2015]	all natural lakes within the administrative boundaries of this region (N=362)
Rocky Mountains of Colorado	calculated from reported N_2O saturation from 26 natural lakes [*McCrackin and Elser*, 2011], average T_{water} estimated from T_{air}, and an estimated k_{600} of 1.16 (based on SWB size after *Read et al.*, 2012)	natural lakes within a 150 km broad band from Niwot Ridge to Molas Pass and minimum altitude of 2,277 m following the site description in *McCrackin and Elser* [2011] (N=67)
Republic of Ireland	reported average N_2O emission rates (head space) from 121 headwater lakes across Republic of Ireland [*Whitfield et al.,* 2011]	natural lakes within the boundaries of Republic of Ireland, with WSL=1 and a maximum watershed area of 4 km^2 and surface areas < 0.5 km^2 following site description in *Whitfield et al.* [2011]
Quebec	average N_2O emission rates from 155 SWBs [*Soued et al.*, 2015]	all SWBs within administrative boundaries of Quebec (N=195,000)
Great Lakes	reported N_2O emission rates from Lake Huron, Lake Erie, and Lake Ontario [*Lemon and Lemon*, 1981]	results from the same large SWBs identified in HydroLAKES by name and location (N=3)

2
3

4   In total, we identified 7 regions from the literature review for which we could compare our

5   simulation results to observation-driven estimates. Table 1 lists for each of these regions the

6   sources and methodology behind the observation-based estimate and the selection of simulation

7   results for comparison. In addition, we compared simulation results against direct observations

8   from three large SWBs: Lake Kivu in East Africa [*Roland et al., 2017*], as well as Lake Poyang

9   [*L. Liu et al., 2013*] and Lake Taihu [*Wang et al., 2009*], which are the two largest freshwater lakes

10   in China. In order to compare our simulation results to observation-driven estimates of N_2O

11   emission rates per area of water surface (in mmol N m^{-2}yr^{-1}), we divided the simulated N_2O

12   emission flux by the water surface area reported in HydroLAKES for each SWB and for both

13   simulations DS1 and DS2.

3 Results

3.1 Model validation

16   Figure 2 compares simulated (DS1 and DS2) vs. observed mean N_2O emission rates per

17   water surface area (N_2O_{em}/A_{water}) for the 7 regions and 3 large SWBs reported in Table 1. Model

18   results correspond to the simulated means using the best estimate for the *EF* (0.9%) and to the

19   range obtained with the lower-bound (0.3%) and upper-bound (1.5%) *EF* values. Table 2 provides

20   the numerical values for the simulated and observed mean and standard deviations of N_2O_{em}/A_{water}

21   rates for each region or large SWB. Overall, we find that our model is able to reproduce the large-

22   scale spatial trends in average N_2O_{em}/A_{water} rates across mid to high latitudes. Moreover, simulated

23   average N_2O emission rates per water surface area for DS2 are relatively close to the observation-

24   driven estimates, while DS1 appears to overestimate average flux rates. Exceptions are the regional

25   estimates for Tianjin region in China and the Republic of Ireland, which are substantially

26   overestimated with both DS1 and DS2. The Tianjin region is highly urbanized and thus the map

27   of estimated N inputs to the inland water network, which we used to calculate TN inflows to lakes,

28   gives particularly high yields. As *Liu et al.* [*2015*] report TN concentrations for their 10 observed

29   lakes in this region, we can further reduce the set of SWBs used for the model-data comparison to

30   those SWBs with a simulated TN concentration that does not exceed their maximum reported TN

31   concentration of 290 μM. Applying this maximum TN concentration, we retain only 141 of the

32   365 SWBs in the Tianjin region. The simulated N_2O_{em}/A_{water} from these 141 SWBs are in fact

33   quite close to those reported by Liu et al. (Fig. 2, Table 2). Similarly, the Irish lakes studied by

34 *Whitfield et al.* [*2011*] are described as oligotrophic, which implies a maximum TN concentration

35 of 26 µM [*Carlson, 1977*; *Kratzer & Brezonik, 1981*]. Applying this value as upper threshold, we

36 only retain 9 of the 350 previously selected SWBs, and the simulated average N_2O_{em}/A_{water} rate is

37 again quite close to the observations by *Whitfield et al.* (Fig. 2, Table 2).

38   As stated in the methods section, a SWB-by-SWB comparison of simulated vs.

39 observation-driven N_2O_{em}/A_{water} rates is a questionable approach. However, for two of the three

40 large SWBs for which we performed this comparison, we find a good agreement between

41 simulated and observation-driven estimates, while N_2O emission from Lake Kivu appear to be

42 overestimated by our model.

43

44 **Table 2.** Regionalized comparison of simulated (best estimate based on EF=0.9%) vs. observation
45 based estimates of N_2O emission rates per water surface area (N_2O_{em}/A_{water}), reported as arithmetic
46 mean rates ±standard deviation. Note that for the Tianjin Region and Ireland, we also report
47 alternative statistics using only SWBs for which the simulated TN concentration do not exceed a
48 threshold value (see text for details).
49

| Region | Mean N_2O_{em}/A_{water} [mmol N m^{-2}yr^{-1}] | | | |
	observed	DS1	DS2	Reference
				Huttunen et al., 2002,
Finland	0.9±3.6	1.2±1.3	0.7±1.1	2003a, 2003b, 2004
Switzerland	10.7±11.9	31.6±22.9	12.2±7.4	*Mengis et al.,* 1997
Tianjin region (China)	0.7±0.1	19.7±25.9	10.4±18.5	*Liu et al.,* 2015
- TN conc. < 290 µM		1.0±1.1	0.7±0.1	-
Rocky Mountains	2.0±0.9	3.7±2.6	2.6±2.1	*McCrackin & Elser,* 2011
Ireland	0.5±0.6	3.5±3.4	2.8±3.0	*Whitfield et al.,* 2011
- TN conc. < 26 µM		1.0±0.5	0.4±0.2	-
Quebec	1.2±3.5	0.8±1.1	0.6±0.8	*Soued et al.,* 2015
Great Lakes	1.2±4.9	3.5±2.2	1.2±0.8	*Lemon & Lemon,* 1981
Lake Kivu (E-Africa)	0.3	5.3	1.5	*Roland et al.,* 2017
Lake Poyang (China)	6.9±3.7	5.2	5.8	*Liu et al.,* 2013
Lake Taihu (China)	4.3	4.4	3.5	*Wang et al.,* 2009
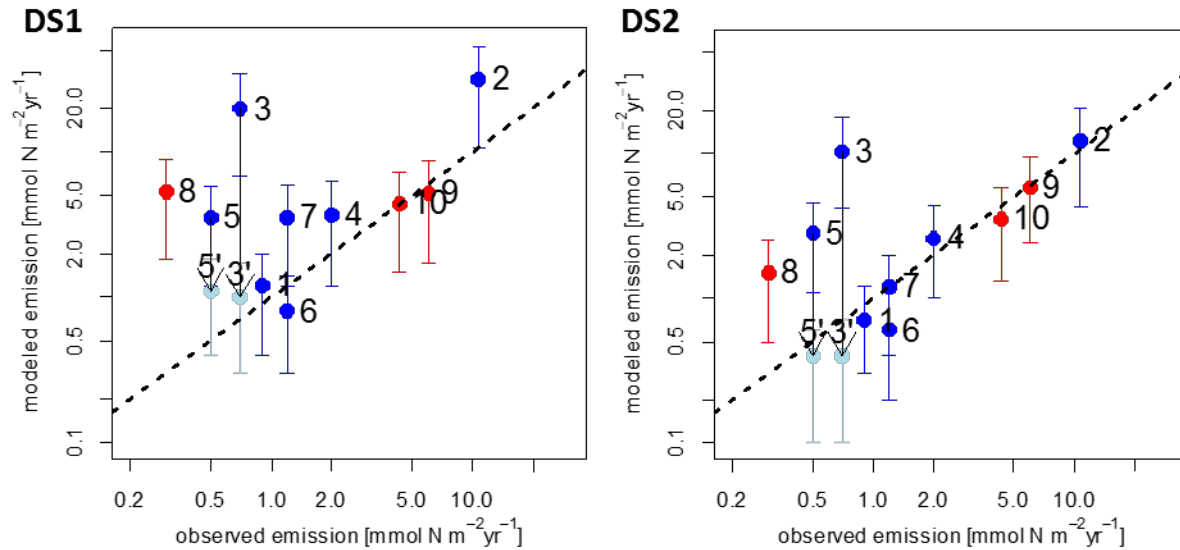
1 – Finland, 2 – Switzerland, 3 – Tianjin Region (China), 4 – Rocky Mountains, 5 – Ireland,
6 – Quebec, 7 – North American Great Lakes, 8 – Lake Kivu (E-Africa), 9 – Lake Poyang (China),
10 – Lake Taihu (China)

50
51 **Figure 2.** Regional averages of observed vs. simulated N_2O emission rates for the two simulation
52 runs DS1 and DS2. The round points correspond to the best model estimates based on an EF=0.9%,
53 the whiskers represent the range defined by alternative lower and upper bound estimates based on
54 *EFs* of 0.3% and 1.5%, respectively. Blue: regions with groups of SWBs; light blue: alternative
55 results for two regions which were constrained by a maximum TN concentration of 26 µM (#5')
56 and 280 µM (#3') as reported in the reference papers (see Table 1); red: single large SWBs. The
57 dashed line represents the 1:1 line. For exact averages and standard deviations in flux rates per
58 region see Table 2.

59

60 **3.2 Patterns of simulated N_2O emissions across space and per type of standing water body**

61   In what follows, we restrict our analysis to results for the more elaborated scenario DS2,

62 which is identified in section 3.1 as the better performing model set-up. At the global scale, we

63 estimate a N_2O emission from SWBs of 4.5±2.9 Gmol N yr^{-1}. The simulated spatial distribution

64 of SWB N_2O emission per continental surface area (N_2O_{em}, Fig. 3a) is mainly following the

65 geographic distribution of these water bodies (Fig. S2a). The simulated spatial patterns of

66 N_2O_{em}/A_{water} rates (Fig. 3b), on the contrary, mainly follow those of TN inputs to the inland water

67 network (Fig. S2b). According to the HydroLAKES database used here, about 44% of the area of

68 SWBs is found at latitudes higher than 50° (here and in the following, latitudinal zonation includes

69 both hemispheres). However, this latitudinal zone contributes only to about 20% of the global

70 SWB N_2O emissions due to low average N_2O emission rates per water surface area resulting from

71   low average TN concentrations compared to other zones (Table 3). The other latitudinal bands

72   (25° – 50° and <25° in Table 3, compare also Fig. 3b) are characterized by higher N_2O_{em}/A_{water}

73   rates. The latitudinal band between 25° and 50° contributes nearly half of the global N_2O emission

74   due to the combination of a large share in SWB surface area and high average N_2O_{em}/A_{water} rates.

75   Latitudes below 25° still contribute about 30% to global emissions despite their low share in global

76   SWB surface area. Summarizing SWB surface areas and N_2O emissions per continent (Table 3),

77   we see a clear dominance of North America and Europe, which together contribute about ¾ of the

78   global SWB area and nearly ½ to global SWB N_2O emissions. In contrast, Australia and South

79   America together contribute only about one tenth of the global flux. Note however that the majority

80   of the SWBs of North America and Europe are concentrated in the less populated, near-natural

81   Boreal zone (>50°) where N_2O emission rates per water surface area are rather low (Fig. 3).

82   Accordingly, the average N_2O_{em}/A_{water} rates on both continents are rather low compared to those

83   estimated for Asia, S-America and Africa (Table 3).

84   Classifying SWBs according to the definitions used in the HydroLAKES database, we

85   estimate global N_2O emissions from natural lakes without dams, natural lakes that are regulated

86   by dams, and reservoirs of 1.8±1.2 Gmol N yr^{-1}, 0.3±0.2 Gmol N yr^{-1}, and 2.4±1.5 Gmol N yr^{-1},

87   respectively (Table 3). Surprisingly, reservoirs contribute 53% of the global lake N_2O emissions

88   although they represent only about 9% of the global SWB area. On the other hand, natural lakes

89   without dam constructions contribute only 40% to global emissions, while they represent 84% of

90   the global SWB surface area. Accordingly, reservoirs show N_2O_{em}/A_{water} rates that are one order

91   of magnitude larger than those for natural lakes with and without dam constructions. As

92   N_2O_{em}/A_{water} from both types of natural lakes are rather similar, and as natural lakes with dam

93   constructions play globally a minor role, we aggregate both types of water bodies in the following

94   simply as natural lakes. The relative contribution of reservoirs to N_2O emissions is highest in the

95   low latitudes (<25°) with 67%, and lowest in the high latitudes (>50°) with only 30%.

96   Table 4 lists the correlations between simulated N_2O_{em}/A_{water} rates, TN concentrations and

97   the environmental drivers used in our modelling approach, which largely explain these spatial

98   patterns. Simulated N_2O_{em}/A_{water} rates show substantial positive correlations to TN inputs (TN_{in}),

99   which is one of the main drivers of our model. This strong correlation explains the high

100   N_2O_{em}/A_{water} rates in the densely populated and/or agriculturally used areas of the temperate zone

101   (Fig. 3b) where inland water TN loads are increased by fertilizer application and sewage water

102   inputs [*Seitzinger et al., 2005*]. We also find a high correlation of simulated N_2O_{em}/A_{water} rates to

103   TP inputs and the watershed area per SWB, which are due to the high correlations between these

104   parameters and TN_{in} . In contrast, we find a significantly negative correlation between

105   N_2O_{em}/A_{water} rates and the water residence time τ_r, although τ_r has by definition a positive effect

106   on the ratio N_2O_{em}/TN_{in} (eq. 9, Fig. 1b). This can be explained by the strong negative correlation

107   of τ_r to TN_{in} as the main driver of simulated N_2O emissions (Table 4). Simulated TN

108   concentrations show a very high correlation to simulated N_2O_{em}/A_{water} rates. This relationship also

109   becomes apparent when comparing the regional differences in both parameters, or when

110   comparing global estimates for natural lakes vs. reservoirs (Table 3).

111
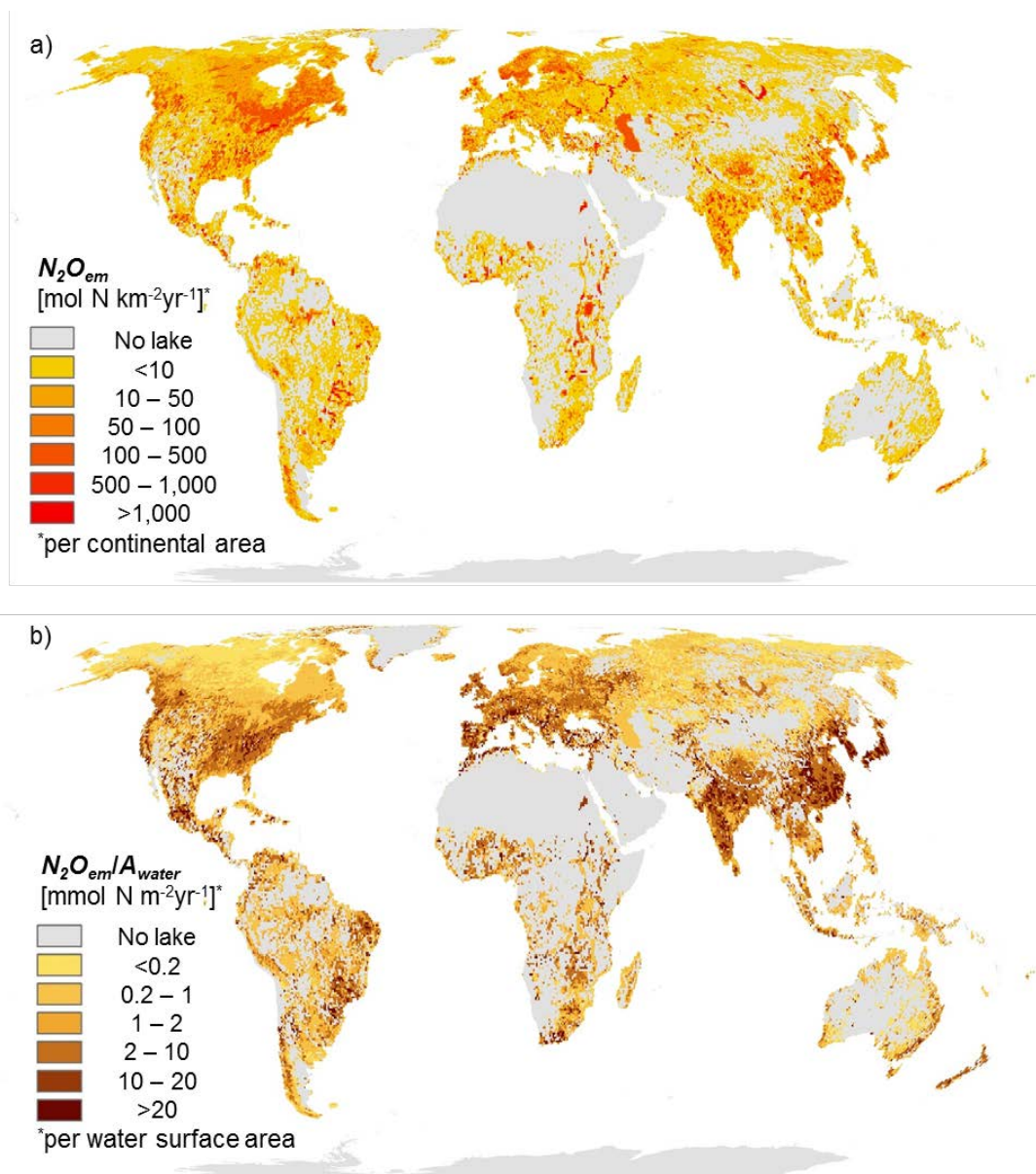
Figure 3. Simulation results of standing water body (natural lakes and reservoirs) N$_2$O emissions (N_2O_{em}) as a) flux densities per continental area, and b) emission rates per water surface area (N_2O_{em}/A_{water}).

117 **Table 3.** Simulated N_2O emissions per latitudinal zone, continent and type of water body. We report the totals of standing water body
118 area (ΣA_{water}) and N_2O emissions (ΣN_2O_{em}), the contribution of reservoirs to ΣA_{water} and ΣN_2O_{em} (*% reservoirs*), the area weighted mean
119 of N_2O emission rates per water surface area ($\Sigma N_2O_{em}/\Sigma A_{water}$), and the arithmetic means of TN concentrations and water residence time
120 τ_r. Note that for TN concentrations, we calculated the mean from the values between 1st and 99th percentile to avoid the effect of single
121 extreme values.

	ΣA_{water} [10^3 km^2]	*% reservoirs*	ΣN_2O_{em} [Gmol N yr^{-1}]	*% reservoirs*	$\Sigma N_2O_{em}/\Sigma A_{water}$ [mmol N m^{2}yr^{-1}]	Mean TN conc. [µM]	Mean τ_r [years]
Estimates by latitudinal band							
< 25°	427	19	1.4±0.9	67	3.3±2.1	173	1.1
25° - 50°	1,201	8	2.1±1.4	54	1.7±1.2	139	3.3
> 50°	1,299	5	0.9±0.6	30	0.7±0.5	20	5.5
Estimates by continent							
Africa	266	13	0.6±0.4	55	2.3±1.5	169	3.6
Asia	216	13	1.2±0.8	69	5.6±3.7	285	5.3
Australia	60	6	0.0±0.0	37	0.0±0.0	66	5.9
Europe	837	7	1.0±0.6	41	1.2±0.7	42	7.3
N-America	1,309	6	1.1±0.7	38	0.8±0.5	26	4.4
S-America	140	26	0.5±0.3	72	3.6±2.1	95	1.6
World	2,927	9	4.5±2.9	53	1.5±1.0	42	4.9
Global estimates by lake type							
Natural lakes	2,677	-	2.1±1.3	-	0.8±0.5	41	4.9
- w./o. dams	2,472	-	1.8±1.2	-	0.7±0.5	41	4.9
- w. dams	205	-	0.3±0.2	-	1.5±1.0	51	12.7
Reservoirs	250	-	2.4±1.5	-	9.6±6.0	165	6.3

122

123 **Table 4.** Pearson correlations of model parameters[*]. All parameters have been log-transformed. All reported correlations are statistically
124 significant at a p=0.05 level.

125

	N_2O_{em}/A_{water}	A_{water}	τ_r	TN conc.	TN_{in}	TP_{in}	A_{wshd}
A_{wshd}	0.53	0.48	-0.73	0.45	0.85	0.88	1.00
TP_{in}	0.78	0.41	-0.76	0.72	0.98	1.00	
TN_{in}	0.83	0.40	-0.76	0.77	1.00		
TN conc.	0.92	0.00	-0.57	1.00			
τ_r	-0.61	0.09	1.00				
A_{water}	0.06	1.00					
N_2O_{em}/A_{water}	1.00						

126

127 [*]A_{wshd} =watershed area, A_{water} = surface area of the standing water body, τ_r = water residence time, TP_{in} = inflow of total phosphorous
128 from upstream, TN_{in} = inflow of total nitrogen from upstream, N_2O_{em}/A_{water} = N$_2$O emission rate per water surface area.

129   **4 Discussion**

130   **4.1 Contribution of natural lakes to inland water N₂O emissions**

131   *Maavara et al.* [2019] gave estimates of N_2O emissions from all water bodies in the GRanD

132   database comprising reservoirs as well as natural lakes regulated by dam construction, which

133   represent the lake type classes 2 and 3 in the HydroLAKES database used here. For the ensemble

134   of these two classes, our global best estimate of 2.7 Gmol N yr^{-1} is slightly lower than the 3.0 Gmol

135   N yr^{-1} given by Maavara et al. [2019] though using a similar model framework. This can be

136   explained by the reduced simulated N inputs to these water bodies resulting from the additional N

137   losses through denitrification and burial in the numerous natural lakes without dam constructions

138   which are accounted for in the present study. In contrast to *Maavara et al.* [2019], we group natural

139   lakes with dam construction and natural lakes together, and analyze their behavior in opposition

140   to reservoirs as man-made water bodies.

141   Nevertheless, global N_2O emissions from reservoirs are slightly higher than those from

142   natural lakes because of higher simulated TN concentrations and N_2O emission rates per lake

143   surface area (N_2O_{em}/A_{water}). These results can be explained by the location of reservoirs, which

144   are often found in more populated or agriculturally impacted areas where the anthropogenic

145   contribution to riverine N loads is substantial [*Deemer et al., 2016*], while a large proportion of

146   natural lakes is found in the more pristine boreal zone [*Messager et al.*, 2016; *Verpoorter et al.*,

147   2014, *Hastie et al.,* 2018]. Also, most natural lakes are regionally concentrated and rather

148   disconnected from the main river network or found in mountainous headwater regions, while many

149   reservoirs are built lower in the river network to serve their particular purposes of storing water

150   from larger rivers for irrigation or hydropower demands. Accordingly, reservoirs have on average

151   larger watershed areas than natural lakes, as reflected by the global averages of 12,853 km^2 vs.

152   617 km^2 [*Messager et al., 2016*], respectively, and thus receive on average higher loads of TN.

153   When additionally taking into account the riverine N_2O emissions of 3.3 Gmol N yr^{-1}

154   [*Maavara et al.,* 2019], we estimate that natural lakes contribute only about ¼ to the global N_2O

155   emission flux from inland waters. Using the recent estimate of global river surface area of 773±79

156   10^3 km^2 [*Allen & Pavelsky, 2018*], the estimated river N_2O emission flux would translate into an

157   area-weighted average rate of 4.3 mmol N m^{-2}yr^{-1} which is again substantially higher than that for

158   natural lakes (0.8±0.5 mmol N m^{-2}yr^{-1}, see Table 3), but lower than the rate of 9.6±6.0 mmol N m^{-}

159 $^2yr^{-1}$ estimated here for reservoirs. This again suggests that reservoirs are predominantly found in
160 areas where riverine N loads are anthropogenically increased.

161   The global scale spatial patterns in N_2O emissions from SWBs found here (Fig. 3) are quite
162 different from those of rivers simulated by *Maavara et al.* [2019]. The spatial patterns depend
163 mainly on the areal distribution of the respective inland water surface, but also on the TN loads
164 (Fig. S2). Latitudes > 50° contribute about 20% to global SWB N_2O emissions and 44% to their
165 surface area, while the contribution of these regions to global river N_2O emission and river surface
166 area are only about 10% and 27%, respectively [*Lauerwald et al., 2015*; *Maavara et al., 2019*].
167 Thus, in comparison to the rest of the globe, the contribution of high latitudes to inland water N_2O
168 emission are disproportionally low compared to their contribution to inland water surface area, a
169 result which can be explained by generally low inland water TN loads (Fig. S2). On the contrary,
170 low latitudes < 25° account for about 70% of global river N_2O emissions [*Maavara et al., 2019*]
171 and 50% of river surface area [*Lauerwald et al., 2015*], but only about 30% and 15% of SWB N_2O
172 emissions and area, respectively (Table 3). Here, the contribution to global inland water N_2O
173 emissions are disproportionally high compared to their share in water surface area, which is related
174 to higher TN loads (Fig. S2). Moreover, the N_2O emission from SWBs in low latitudes are
175 dominated by reservoirs, which contribute about two third of the total flux and one fifth of the
176 SWB surface area in that latitudinal band.

4.2 Comparison with previous studies

178   To our knowledge, our study is the first to give a global, spatially explicit estimate of N_2O
179 emissions from SWBs, and further the first study to give separate estimates for natural lakes and
180 reservoirs in a consistent manner. However, a few global estimates have been published in recent
181 years, either on N_2O emission from standing waters without distinguishing natural lakes from
182 reservoirs [*Soued et al.*, 2015, *DelSontro et al.*, 2018], or from reservoirs only [*Deemer et al.*,
183 2016]. In Table 5, we compare those estimates to our own simulation results. The results vary due
184 to different methods of estimation but also due to different estimates or datasets of standing water
185 surface area (A_{water}) used. The simplest method to estimate global fluxes is the upscaling based on
186 averaged, observation-based N_2O_{em}/A_{water} rates which are then multiplied by estimates of total
187 A_{water} [*Deemer et al.*, 2016, *Soued et al.*, 2015, *DelSontro et al.*, 2018]. Using this method,
188 *DelSontro et al.* [2018] estimated a N_2O emission flux from SWBs of 11.4 to 19.3 Gmol N yr^{-1}

189   based on three different estimate of water surface area. These estimates are a factor 2 to 4 higher

190   than our estimate of 4.5 (1.7-7.4) Gmol N yr^{-1}. *Soued et al.* [2015] performed an upscaling for

191   three latitudinal zones, and then summed up the N_2O emission flux estimates to a global value of

192   45.0±21.1 Gmol N yr$^{-,1}$ which is even about 10 times higher than our estimate. Note however that

193   *Soued et al.* [2015] attribute more than 80% of this global estimate to the latitudinal band <25°

194   (Table 5). For this latitudinal band, they derived an average N_2O_{em}/A_{water} rate of 47.2 mmol N

195   m^{-2}yr^{-1} which is more than 20 times higher than the average flux rates found for the other two

196   latitudinal bands (Table 5), and which is based on observations from only 6 reservoirs in Latin

197   America (4xBrazil, 1xPanama, 1xFrench Guiana) taken from the study of *Guérin et al.* [*2008*].

198   Natural tropical lakes have thus not been taken into account in the *Soued et al.* study. Note further

199   that for three of these reservoirs a N_2O_{em}/A_{water} rate of 5.1 mmol N m^{-2}yr^{-1} or lower is reported,

200   while for the other three the reported N_2O_{em}/A_{water} rate is 67.9 mmol N m^{-2}yr^{-1} or higher. This

201   reveals that not all reservoirs in that area show similarly elevated N_2O_{em}/A_{water} rates and highlights

202   the huge uncertainty related to an empirical approach based on very few local measurements. High

203   N_2O emission from tropical reservoirs can be due to the high organic matter content in the

204   submerged soils [*Guérin et al., 2008*], and decreasing greenhouse gas emission with increasing

205   age of reservoirs have been reported [*Barros et al., 2011*] as concentration and reactivity of the

206   submerged organic matter decrease with time [*Maavara et al.*, 2017]. In a recent study on small

207   reservoirs in tropical Africa [*Okuku et al., 2019*], much lower N_2O_{em}/A_{water} rates of 0.7-1.2 mmol

208   N m^{-2}yr^{-1} have been reported, referring to a low organic matter content of submerged soils as

209   explanation. Submerged soils as sources of N_2O do not play a role for natural lakes. Moreover, the

210   low N_2O_{em}/A_{water} rate for Lake Kivu (0.3 mmol N m^{-2}yr^{-1}, Table 2), which is based on an intensive

211   sampling campaign [*Roland et al., 2017*], suggests that tropical lakes are generally not strong

212   sources of N_2O.

213

214

215 **Table 5**: Comparison of results with earlier global and zonal estimates of N_2O emissions from
216 natural lakes and reservoirs or from reservoirs only. For each estimate, the total water surface area
217 (ΣA_{water}) and the total N_2O emission flux (ΣN_2O_{em}) are reported. For the upscaling studies cited
218 below, the $\Sigma N_2O_{em}/\Sigma A_{water}$ represents the average observed N_2O emission rate per water surface
219 area which was multiplied by ΣA_{water} to estimate ΣN_2O_{em}. Where ΣN_2O_{em} was estimated based
220 on statistical and process based models (such as in the present study), $\Sigma N_2O_{em}/\Sigma A_{water}$ was
221 calculated for comparison. For studies based on upscaling of observations or statistical models,
222 the number of observations N is indicated.

Reference	N	$\Sigma N_2O_{em}/\Sigma A_{water}$ [mmol N m^{-2}yr^{-1}]	ΣA_{water} [10^6 km^2]	ΣN_2O_{em} [Gmol N yr^{-1}]
Lakes and reservoirs, global				
DelSontro et al. [2018], upscaling	309	3.5	4.45[1]	15.7
"	"	3.6	5.36[2]	19.3
"	"	3.5	3.23[3]*	11.4
DelSontro et al. [2018], statistic model (R^2=0.09)	268	4.8 (3.1-7.2)[a]	4.45[1]	21.4 (13.6-32.1)[a]
"	"	5.1 (3.2-7.4)[a]	5.36[2]	27.1 (17.1-39.9)[a]
"	"	5.8 (3.5-8.4)[a]	3.23[3]*	18.6 (11.4-27.1)[a]
Soued et al. [2015], upscaling based on latitudinal zones (see below)	298	10.7	4.20[1]	45.0±21.1[b]
This study	-	1.5±1.0[c]	2.93[3]	4.5±2.9[c]
Lakes and reservoirs, high latitudes (>54°)				
Soued et al. [2015], upscaling based on literature data	14	0.8	1.93[1]	1.6±0.6[b]
Soued et al. [2015], upscaling based on observations from Quebec	155	2.4	1.93[1]	4.7±0.4[b]
This study	-	0.5±0.3[c]	1.03[3]	0.5±0.3[c]
Lakes and reservoirs, mid latitudes (25°-54°)				
Soued et al. [2015], upscaling	137	2.5	1.45[1]	3.6±3.4[b]
This study	-	1.7±1.1[c]	1.47[3]	2.5±1.6[c c]
Lakes and reservoirs, low latitudes (<25°)				
Soued et al. [2015], upscaling	6	47.2	0.77[1]	36.4±17.4[b]
This study	-	3.3±2.1[c]	0.43[3]	1.4±0.9[c]
Reservoirs only, global				
Deemer et al. [2016], upscaling	58	7.8	0.31[4]	2.4
This study	-	9.6±6.0	0.25[3]	2.4±1.5[c]

223 [1]after *Downing et al.* [*2006*]; [2]after *Verporter et al.* [*2014*]; [3]after *Messager et al.* [*2016*]; [4]after *Lehner et al.* [*2011*]
224 *[*]DelSontro et al.* used scaling laws inspired by *Downing et al. (2006)* to estimate area of smaller water bodies not
225 represented in HydroLAKES
226 [a]95% confidence interval from statistical model; [b]standard error; [c]value range based on lower bound and upper bound
227 emission factor of 0.3% and 1.5%, respectively (see text).
228

229   Interestingly, our global simulation results for N_2O emission from reservoirs only of

230   2.4±1.5 Gmol N yr^{-1} are actually very close to the upscaling-based estimate *by Deemer et al.* [2016]

231   of 2.4 Gmol N yr^{-1} (Table 5). That finding, together with the regionalized validation of our

232   simulation results against observation based flux estimates for natural lakes (section 3.1), is

233   supportive of our model-based approach. It thus represents an important methodological

234   alternative to empirically based upscaling studies. *DelSontro et al.* [2018] explored an intermediate

235   approach by applying a regression equation to predict N_2O emission rates from lake/reservoir size

236   and chlorophyll-a concentrations. The predicted global emissions are roughly 40-60% higher than

237   those derived from their simple upscaling approach (Table 5). However, given the low predictive

238   power of that equation (R^2=0.09), it is difficult to conclude which of the two methodologies is the

239   most reliable for upscaling. Moreover, even if chlorophyll-a concentrations may be related to

240   organic matter availability and N availability via N fixation by cyanobacteria while lake size may

241   increase the organic matter degradation time, these two parameters are not directly linked with

242   nitrification and denitrification rates. On the contrary, some findings suggest that nitrification and

243   denitrification are actually negatively affected by the presence of algae [*Enrich-Prast et al., 2016*;

244   *Risgaard-Petersen, 2003*]. This lack of mechanistic connection could explain the low predictive

245   power of the empirical equation by *DelSontro et al.* [2018].

246

4.3 Model limitations and challenges for future developments

248   In our study, we estimated N_2O emissions from global SWBs based on simulated TN and

249   TP flows through each SWB and the residence time τ_r within each SWB, using the model

250   framework developed by *Maavara et al.* [2019]. This model framework allows to estimate annual

251   nitrification and denitrification fluxes, and uses *EFs* to estimate N_2O production from these fluxes,

252   a methodology so far mainly applied to rivers. To estimate N_2O emissions, we followed two

253   scenarios. The first rather simplistic scenario (DS1) assumes N_2O emission to equal N_2O

254   production. The other scenario (DS2) accounts for a reduced net-production of N_2O in the process

255   of denitrification due to the reduction of N_2O to N_2, which becomes significant at water residence

256   times longer than 7 months. For the 37% of the 1.4 million SWBs which have τ_r of 7 months or

257   less, the global emissions estimated by model configurations DS1 and DS2 are nearly identical at

258   2.0 Gmol N yr^{-1}. *Maavara et al.* [2019] also found that DS1 and DS2 gave very similar results for

259   rivers, where τ_r is generally low and gas exchange is quick For the remaining SWBs with a higher

260   τ_r, the scenario DS1 would give a total N_2O emission flux which is more than twice than that

261   simulated under DS2. In our model validation against observation based flux estimates, we found

262   that simulation of N_2O emissions under DS2 performs better, and concluded that the reduced net-

263   production of N_2O from denitrification at higher residence times is a non-negligible process in

264   SWBs, which precludes the use of constant *EFs* as done for rivers [e.g. *Beaulieu et al., 2011*; *Hu*

265   *et al., 2016*; *Seitzinger et al., 2000*].

266   A considerable source of uncertainty in our global model results is related to the three

267   drivers used: TN and TP inputs to the lakes and reservoirs and τ_r of the lakes and reservoirs. We

268   thus performed additional simulations quantifying the sensitivity of our global SWB N_2O emission

269   estimate to those three drivers by systematically varying each driver individually. When increasing

270   or decreasing TN inputs from the watershed by 50%, the simulated global N_2O emission is

271   increased or decreased by 44%, respectively. Increasing or decreasing TP inputs from the

272   watershed by 50% increases or decreases simulated emissions by 6%, respectively, which is due

273   to the effect of TP/TN ratios in the water column on the simulated fixation rates of atmospheric N

274   (eq. 4), and is thus a secondary effect on the total inputs of TN to SWBs. Finally, increasing τ_r by

275   50% leads to an increase in simulated N_2O emissions of 11%, while a decrease of τ_r by 50% leads

276   to a decrease in simulated N_2O emission by 16%. The relatively low sensitivity of global N_2O

277   emission estimates to τ_r can be explained by the fact that the ratio between N_2O emission to TN

278   inputs reaches its maximum already at a τ_r of about one year (Fig. 1b), while nearly half of the 1.4

279   million SWBs of the HydroLAKES database have a higher τ_r. Finally, as revealed by the bounds

280   in N_2O emissions calculated using alternative *EFs* of 0.3% and 1.5%, we see that our estimates of

281   N_2O emissions are most sensitive to the value of this parameter, with emissions changing nearly

282   proportionally to the chosen *EF*.

283   As drivers of our model, TN inputs from upstream and τ_r are not easy to determine and

284   thus usually not reported in empirical studies. On the contrary, the concentrations of TN or

285   important N-species like nitrate are often reported and are important variables as *Deemer et al.*

286   [2016], for instance, report a strong correlation between observed N_2O flux rates and nitrate

287   concentrations (R^2=0.49). Similar correlations have been reported at regional scale for natural

288   lakes [*McCrackin & Elser, 2011*]. Consistent with these observations, our simulation results also

289   reproduce a high correlation between TN concentrations and N_2O emission rates (R^2=0.85, Table

290   4). For the entirety of SWBs in our study, we calculate an mean (±standard deviation) TN

291   concentration of 42±75 µM (based on values between 1th and 99th percentile to exclude the effects

292   of outliers, Table 3) which is actually very close to the observation-based estimate of global natural

293   lake and reservoir TN concentrations of 38±186 µM by Chen et al. [*2015*]. That means that on

294   global average, our simulated TN concentrations are reasonable, and not the source for a general

295   under- or overestimation of N_2O emissions.

296   Our use of TN as substrates for N_2O production, as opposed to using dissolved inorganic

297   nitrogen only [*Kroeze et al., 2005*; *Seitzinger et al., 2000*], is justified by the fact that both organic

298   and inorganic N play an important role in aquatic N cycling. Inorganic N (e.g. NH_4^+, NO_2^- and

299   NO_3^-) concentrations represent only the direct availability of substrates for nitrification and

300   denitrification. The aerobic or anaerobic degradation of organic nitrogen will result in the in-situ

301   release of NH_4^+ that can be oxidized to NO_2^- and NO_3^- via nitrification and will potentially release

302   N_2O, depending on oxygen concentrations. Both NO_2^- and NO_3^- produced aerobically by

303   nitrification can subsequently be reduced to N_2O via denitrification, at low oxic conditions

304   [*Fenchel et al., 1998*].

305   At regional scale, however, large uncertainties may result from the global scale modelling

306   approach. The examples of the Irish headwater lakes and lakes in the Tianjin region (China)

307   discussed in section 3.1 illustrate that while the model is able to reproduce observed N_2O emission

308   rates given correct TN loads, the coarse representation of TN inputs from point and non-point

309   sources (0.5° ≈ 50 km) is a considerable source of uncertainty in our simulations. In particular for

310   small lakes with small watershed areas this may lead to a wrong attribution of TN loads. While

311   strong point-sources of TN associated with urban areas are important for the TN loads of larger

312   rivers, they are in reality likely not linked to small lakes. Similarly, small oligotrophic head water

313   lakes in an otherwise agriculturally impacted region will not be represented at this spatial

314   resolution. Based on these considerations, our modelling approach may overestimate TN loads and

315   thus N_2O emissions from small lakes in agricultural and urban areas.

316   Another source of uncertainty is the representation of natural lakes and reservoirs at global

317   scale. As seen from table 5, different global estimates of SWB N_2O emissions depend on different

318   estimates of the number and total area of SWBs. The HydroLAKES database used here considers

319   only natural lakes and reservoirs with a surface area ≥0.1 km^2, and thus gives lower estimates of

320   SWB surface area than the estimates by *Downing et al.* [2006] and *Verpoorter et al.* [2014].

321   *Downing et al.* [*2006*] used statistics to estimate the number of small lakes and reservoirs not

322 represented in global databases. *Verpoorter et al.* [2014] used high-resolution satellite data to map

323 areas of standing water bodies as small as 0.002 km^2. However, the *Verpoorter et al.* study relied

324 on an automated classification algorithm and ground truthing was only performed for Sweden,

325 thus questioning its reliability for global scale applications. Nevertheless, we may underestimate

326 the global N$_2$O emissions from SWBs, as we do not account for water bodies smaller than 0.1km^2.

327 The underestimation is likely highest for high latitudes were small glacial lakes are numerous. This

328 is supported by the total SWB surface area for latitudes >54° reported by *Soued et al.* [2015] on

329 the basis of the work by *Downing et al.* [2006], which is nearly twice our estimate (Table 5).

330   Finally, an additional source of uncertainty is the necessary simplicity of our model, which

331 simulates SWB N cycling and N$_2$O emission rates at the annual time-scale and which, describes

332 each SWB only through the variable τ_r for the spatially explicit upscaling step. The water column

333 and aquatic sediments are not explicitly represented, but simulated N transformation rates,

334 including the production of N$_2$O, integrate processes in both media. SWBs, however, are

335 heterogeneous ecosystems with an intrinsic spatial and temporal variability in the different

336 processes of N cycling. *Mengis et al.* [*1997*] and *Beaulieu et al.* [*2015*] have described sources and

337 sinks of N$_2$O for stratified SWBs varying in morphology and trophic status. Generally, in the well-

338 mixed and oxic upper layer, the epilimnion, but also in the oxic parts of the lower layer, the

339 hypolimnion, nitrification is the dominant source of N$_2$O. In anoxic parts of the hypolimnion,

340 denitrification is the dominant process, which can be source as well as sink for N$_2$O. *Mengis et al.*

341 [*1997*] found for deep Swiss lakes that this anoxic part of the water column is often undersaturated

342 with respect to atmospheric N$_2$O, which clearly indicates a net-consumption of N$_2$O through

343 denitrification. Moreover, *Beaulieu et al.* [2015] found for a group of reservoirs in Ohio that

344 denitrification in the anoxic hypolimnion is a sink for N$_2$O at nitrate concentrations below 3.6 μM,

345 while at higher nitrate concentrations denitrification is a source of N$_2$O. *Beaulieu et al.* explain

346 that observation by the low energy yield for the reduction of N$_2$O to N$_2$ compared to the reduction

347 of nitrate, thus favoring full reduction only when the availability of nitrate is limited. High peaks

348 of N$_2$O in the water column have also been reported at the oxic-anoxic interface, mainly resulting

349 from high nitrification rates sustained by underlying ammonia-rich anoxic waters [*Beaulieu et al.,*

350 *2015*; *Mengis et al., 1997*; *Roland et al., 2017*]. Conversely, nitrification of ammonia in the oxic

351 top layers can be the main source of nitrate for denitrification in the lower layer, as observed in

352 aquatic sediments [*Liikanen et al., 2003*; *Zhu et al., 2015*]. Aquatic sediments as sources for lake

353　N$_2$O emission have mainly been reported for eutrophic and shallow SWBs, and in particular for

354　shallower parts of the SWB [*Liikanen et al., 2003*; *Zhu et al., 2015*]. In terms of temporal

355　dynamics, only the epilimnion exchanges gas with the atmosphere during periods of thermal

356　stratification. Therefore, periods of lake turnover have been reported to represent hot moments of

357　nitrification, N$_2$O production and emission as anoxic water rich in ammonium mix with oxic

358　waters [*Beaulieu et al., 2015*; *Roland et al., 2017*]. Temporal (and spatial) variations in N$_2$O

359　emissions have also been reported to be related to algae blooms and the associate increase in

360　nitrification rates [*Liu et al., 2018*]. However, while the global coverage with direct observations

361　of SWB N$_2$O emission is already poor, studies systematically investigating their seasonal pattern,

362　i.e. during all phases of lake mixing and aquatic growing season, are even scarcer.

363　　　　More systematic fieldwork is thus needed to better understand the annual and seasonal N$_2$O

364　budgets of natural lakes and reservoirs, and to better constrain their contribution to atmospheric

365　N$_2$O budgets at global scale. This scientific progress should be aided by the development and

366　application of more sophisticated models, in particular for the global scale upscaling of N$_2$O

367　emission estimates. Future models should represent these N processes and the individual N-species

368　(N$_2$O, N$_2$, ammonium, nitrite, nitrate, dissolved organic N and particulate organic N) in a spatially

369　resolved framework, distinguishing processes in benthic sediments and in the water column, and

370　further processes in the littoral and pelagic zones of SWBs, while taking into account stratification

371　and the geometry of the SWB bed. Such a model should further represent interactions of N-

372　processes with the organic C cycling and lake pH [*Bajwa et al., 2006*; *Kowalchuk & Stephen,*

373　*2001*]. In particular the dynamics of N$_2$O sources and sinks have to be represented more explicitly

374　to replace the use of empirical *EFs*. Moreover, the models will have to resolve the seasonal cycle,

375　representing the growing season of aquatic vegetation and distinguishing periods of SWB

376　stratification and turnover. To realize that, the representation of biogeochemical processes should

377　be coupled to models of SWB physics driven by temporally resolved climate forcing data, like for

378　instance the FLake model [*Thiery et al., 2014*]. Validation of these models will require empirical

379　studies describing the physical and biogeochemical mechanisms of N and N$_2$O cycling for a broad

380　range of SWBs of different morphology, trophic status and climate-induced mixing regimes.

381

5 Conclusions

382

383 Using a two-step modeling approach based on a mechanistic N model and predictive

384 equations for spatially explicit upscaling, we re-estimated global N_2O emissions from standing

385 water bodies (natural lakes and reservoirs) at 4.5 ± 2.9 Gmol N yr^{-1}, at the far lower end of existing

386 estimates. Moreover, our results show that reservoirs as man-made lakes contribute more than half

387 of that flux, although they represent less than 9% of the total SWB area. We conclude that natural

388 lakes are a relatively small contributor to global inland water N_2O emissions, even though their

389 global surface area is ca. ten times larger than that of reservoirs and about four times larger than

390 that of streams and rivers. While our approach is admittedly coarse, it still helps to improve our

391 understanding of global inland water N_2O emissions beyond what can be achieved by direct

392 upscaling of averaged observational data or by applying empirically derived relationships such as

393 the one relating N_2O emissions to chlorophyll-a concentrations and SWB size. Our results, despite

394 bearing significant uncertainties resulting from limited available observations and fragmentary

395 knowledge about N cycling in SWBs from a global perspective, is an important step forward as it

396 provides the first spatially explicit estimate of N_2O emissions for 1.4 million SWBs. Further

397 progress in this research field would benefit greatly from improved inland water databases

398 containing smaller water bodies, from a more detailed datasets of N sources to the inland water

399 network at higher spatial resolution and from more fieldwork on SWB N- and N_2O cycling to

400 improve our mechanistic understanding of these processes on regional to global scales.

410 Supporting Information. The simulated lake and reservoir N₂O emission rates at 0.5 degree

411 resolution can be downloaded from https://doi.pangaea.de/10.1594/PANGAEA.900565.

References

413 Allen, G. H., & Pavelsky, T. M. (2018). Global extent of rivers and streams. Science, 361(6402),
414   585 LP – 588, doi: 10.1126/science.aat0636.

415 Bajwa, K. S., Aneja, V. P., & Pal Arya, S. (2006). Measurement and estimation of ammonia
416   emissions from lagoon–atmosphere interface using a coupled mass transfer and chemical
417   reactions model, and an equilibrium model. Atmospheric Environment, 40, 275–286, doi:
418   10.1016/j.atmosenv.2005.12.076

419 Barros, N., Cole, J. J., Tranvik, L. J., Prairie, Y. T., Bastviken, D., Huszar, V. L. M., et al. (2011).
420   Carbon emission from hydroelectric reservoirs linked to reservoir age and latitude. Nature
421   Geoscience, 4(9), 593–596,

422 Beaulieu, J. J., Tank, J. L., Hamilton, S. K., Wollheim, W. M., Hall Jr., R. O., Mulholland, P. J.,
423   et al. (2011). Nitrous oxide emission from denitrification in stream and river networks.
424   Proceedings of the National Academy of Sciences of the United States of America, 108(1),
425   214–219, doi: 10.1073/pnas.1011464108

426 Beaulieu, J. J., Nietch, C. T., & Young, J. L. (2015). Controls on nitrous oxide production and
427   consumption in reservoirs of the Ohio River Basin. Journal of Geophysical Research:
428   Biogeosciences, 120(10), 1995–2010, doi: 10.1002/2015JG002941

429 Bouwman, A. F., Beusen, A. H. W., & Billen, G. (2009). Human alteration of the global nitrogen
430   and phosphorus soil balances for the period 1970-2050. Global Biogeochemical Cycles,
431   23(4), doi: 10.1029/2009GB003576

432 Carlson, R. E. (1977). A trophic state index for lakes. Limnology and Oceanography, 22(2),
433   361–369, doi: 10.4319/lo.1977.22.2.0361

434 Chen, M., Zeng, G., Zhang, J., Xu, P., Chen, A., & Lu, L. (2015). Global Landscape of Total
435   Organic Carbon, Nitrogen and Phosphorus in Lake Water. Scientific Reports, 5, 15043,
436   Retrieved from https://doi.org/10.1038/srep15043

437 Ciais, P., Sabine, C., Bala, G., Bopp, L., Brovkin, V., Canadell, J., et al. (2013). Carbon and
438   Other Biogeochemical Cycles. In T. F. Stocker, D. Qin, G.-K. Plattner, M. Tignor, S. K.
439   Allen, J. Boschung, et al. (Eds.), Climate Change 2013: The Physical Science Basis.
440   Contribution of Working Group I to the Fifth Assessment Report of the Intergovernmental

441   Panel on Climate Change. Cambridge, United Kingdom and New York, NY, USA:
442   Cambridge University Press

443   Deemer, B. R., Harrison, J. A., Li, S., Beaulieu, J. J., DelSontro, T., Barros, N., et al. (2016).
444   Greenhouse Gas Emissions from Reservoir Water Surfaces: A New Global Synthesis.
445   BioScience, 66(11), 949–964, doi: 10.1093/biosci/biw117

446   DelSontro, T., Beaulieu, J. J., & Downing, J. A. (2018). Greenhouse gas emissions from lakes
447   and impoundments: Upscaling in the face of global change. Limnology and Oceanography
448   Letters, 3(3), 64–75, doi: 10.1002/lol2.10073

449   Downing, J. A., Cole, J. J., Duarte, C. M., Middelburg, J. J., Melack, J. M., Prairie, Y. T., et al.
450   (2012). Global abundance and size distribution of streams and rivers. INLAND WATERS,
451   2(4), 229–236, doi: 10.5268/IW-2.4.502

452   Van Drecht, G., Bouwman, A. F., Harrison, J., & Knoop, J. M. (2009). Global nitrogen and
453   phosphate in urban wastewater for the period 1970 to 2050. Global Biogeochemical Cycles,
454   23(3), doi: 10.1029/2009GB003458

455   Enrich-Prast, A., Figueiredo, V., De Esteves, F. A., & Nielsen, L. P. (2016). Controls of
456   sediment nitrogen dynamics in tropical coastal lagoons. PLoS ONE, 11(5), doi:
457   10.1371/journal.pone.0155586

458   Fenchel, T., King, G., & Blackburn, T. (1998). Bacterial biogeochemistry: the ecophysiology of
459   mineral cycling (2nd ed.). London: Academic Press,Fick, S. E., & Hijmans, R. J. (2017).
460   WorldClim 2: new 1-km spatial resolution climate surfaces for global land areas.
461   International Journal of Climatology, 37(12), 4302–4315, doi: 10.1002/joc.5086

462   Fluet-Chouinard, E., Messager, M. L., Lehner, B., & Finlayson, C. M. (2016). Freshwater Lakes
463   and Reservoirs BT - The Wetland Book: II: Distribution, Description and Conservation. In
464   C. M. Finlayson, G. R. Milton, R. C. Prentice, & N. C. Davidson (Eds.) (pp. 1–18).
465   Dordrecht: Springer Netherlands, doi: 10.1007/978-94-007-6173-5_201-1

466   Guérin, F., Abril, G., Tremblay, A., & Delmas, R. (2008). Nitrous oxide emissions from tropical
467   hydroelectric reservoirs. Geophysical Research Letters, 35(6), doi: 10.1029/2007GL033057

468   Hu, M., Chen, D., & Dahlgren, R. A. (2016). Modeling nitrous oxide emission from rivers: a
469   global assessment. Global Change Biology, 22(11), 3566–3582, doi: 10.1111/gcb.13351

470   Huttunen, J. T., Väisänen, T. S., Heikkinen, M., Hellsten, S., Nykänen, H., Nenonen, O., &
471   Martikainen, P. J. (2002). Exchange of CO2, CH4 and N2O between the atmosphere and
472   two northern boreal ponds with catchments dominated by peatlands or forests. Plant and
473   Soil, 242(1), 137–146, doi: 10.1023/A:1019606410655

474   Huttunen, J. T., Alm, J., Liikanen, A., Juutinen, S., Larmola, T., Hammar, T., et al. (2003). Fluxes
475   of methane, carbon dioxide and nitrous oxide in boreal lakes and potential anthropogenic

476   effects on the aquatic greenhouse gas emissions. Chemosphere, 52(3), 609–621, doi:
477   10.1016/S0045-6535(03)00243-1

478 Huttunen, J. T., Juutinen, S., Alm, J., Larmola, T., Hammar, T., Silvola, J., & Martikainen, P. J.
479   (2003). Nitrous oxide flux to the atmosphere from the littoral zone of a boreal lake. Journal
480   of Geophysical Research D: Atmospheres, 108(14), ACH 7-1-ACH 7-10.

481 Huttunen, J. T., Hammar, T., Manninen, P., Servomaa, K., & Martikainen, P. J. (2004). Potential
482   springtime greenhouse gas emissions from a small southern boreal lake (Keihäsjärvi,
483   Finland). Boreal Environment Research, 9(5), 421–427.

484 Kowalchuk, G. A., & Stephen, J. R. (2001). Ammonia-oxidizing bacteria: A model for molecular
485   microbial ecology. Annual Review of Microbiology, doi: 10.1146/annurev.micro.55.1.485

486 Kratzer, C. R., & Brezonik, P. L. (1981). A Carlson-type trophic state index for nitrogen in
487   Florida lakes. JAWRA Journal of the American Water Resources Association, 17(4), 713–
488   715, doi: 10.1111/j.1752-1688.1981.tb01282.x

489 Kroeze, C., Dumont, E., & Seitzinger, S. P. (2005). New estimates of global emissions of N_2O
490   from rivers and estuaries. Environmental Sciences, 2(2–3), 159–165, doi:
491   10.1080/15693430500384671

492 Kroeze, C., Dumont, E., & Seitzinger, S. (2010). Future trends in emissions of N_2O from rivers
493   and estuaries. Journal of Integrative Environmental Sciences, 7(sup1), 71–78, doi:
494   10.1080/1943815X.2010.496789

495 Lauerwald, R., Laruelle, G. G., Hartmann, J., Ciais, P., & Regnier, P. A. G. (2015). Spatial
496   patterns in CO_2 evasion from the global river network. Global Biogeochemical Cycles,
497   29(5), 534–554, doi: 10.1002/2014GB004941

498 Lehner, B., & Döll, P. (2004). Development and validation of a global database of lakes,
499   reservoirs and wetlands. Journal of Hydrology, 296(1–4), 1–22, doi:
500   10.1016/j.jhydrol.2004.03.028

501 Lehner, B., Verdin, K., & Jarvis, A. (2008). New global hydrography derived from spaceborne
502   elevation data. Eos, Transactions, AGU, 89(10), 93–94.

503 Lehner, B., Liermann, C. R., Revenga, C., Vörömsmarty, C., Fekete, B., Crouzet, P., et al.
504   (2011). High-resolution mapping of the world's reservoirs and dams for sustainable river-
505   flow management. Frontiers in Ecology and the Environment, 9(9), 494–502.

506 Lemon, E., & Lemon, D. (1981). Nitrous oxide in fresh waters of the Great Lakes Basin1.
507   Limnology and Oceanography, 26(5), 867–879, doi: 10.4319/lo.1981.26.5.0867

508 Liikanen, A., Huttunen, J. T., Murtoneimi, T., Tanskanen, H., Väisänen, T., Silvola, J., et al.
509   (2003). Spatial and seasonal variation in greenhouse gas and nutrient dynamics and their

510   interactions in the sediments of a boreal eutrophic lake. Biogeochemistry, 65(1), 83–103,
511   doi: 10.1023/A:1026070209387

512   Liu, D., Zhong, J., Zheng, X., Fan, C., Yu, J., & Zhong, W. (2018). N_2O fluxes and rates of
513   nitrification and denitrification at the sediment-water interface in Taihu Lake, China. Water
514   (Switzerland), 10(7), doi: 10.3390/w10070911

515   Liu, L., Xu, M., Lin, M., & Zhang, X. (2013). Spatial variability of greenhouse gas effluxes and
516   their controlling factors in the Poyang lake in China. Polish Journal of Environmental
517   Studies, 22(3), 749–758.

518   Liu, X.-L., Bai, L., Wang, Z.-L., Li, J., Yue, F.-J., & Li, S.-L. (2015). Nitrous oxide emissions
519   from river network with variable nitrogen loading in Tianjin, China. Journal of Geochemical
520   Exploration, 157, 153–161, doi: 10.1016/j.gexplo.2015.06.009

521   Maavara, T, Dürr, H. H., & Van Cappellen, P. (2014). Worldwide retention of nutrient silicon by
522   river damming: From sparse data set to global estimate. Global Biogeochemical Cycles. doi:
523   10.1002/2014GB004875

524   Maavara, T., Parsons, C. T., Ridenour, C., Stojanovic, S., Dürr, H. H., Powley, H. R., & Van
525   Cappellen, P. (2015). Global phosphorus retention by river damming. Proceedings of the
526   National Academy of Sciences, doi: 10.1073/pnas.1511797112

527   Maavara, Taylor, Lauerwald, R., Regnier, P., & Cappellen, P. Van. (2017). Global perturbation
528   of organic carbon cycling by river damming. Nature Communications, 8. doi:
529   10.1038/ncomms15347

530   Maavara, T., Lauerwald, R., Laruelle, G., Akbarzadeh, Z., Bouskill, N., Van Cappellen, P., &
531   Regnier, P. (2019). Nitrous oxide emissions from inland waters: Are IPCC estimates too
532   high? Global Change Biology, 25(2), 473–488, doi: 10.1111/gcb.14504

533   Mayorga, E., Seitzinger, S. P., Harrison, J. A., Dumont, E., Beusen, A. H. W., Bouwman, A. F.,
534   et al. (2010). Global Nutrient Export from WaterSheds 2 (NEWS 2): Model development

535   and implementation. Environmental Modelling & Software, 25(7), 837–853, doi:
536   10.1016/j.envsoft.2010.01.007

537   McCrackin, M. L., & Elser, J. J. (2011). Greenhouse gas dynamics in lakes receiving
538   atmospheric nitrogen deposition. Global Biogeochemical Cycles, 25(4), doi:
539   10.1029/2010GB003897

540   Mengis, M., Gächter, R., & Wehrli, B. (1997). Sources and sinks of nitrous oxide N_2O in deep
541   lakes. Biogeochemistry, 38(3), 281–301, doi: 10.1023/A:1005814020322

542   Messager, M. L., Lehner, B., Grill, G., Nedeva, I., & Schmitt, O. (2016). Estimating the volume
543   and age of water stored in global lakes using a geo-statistical approach. Nature
544   Communications, 7, 13603.

545   Okuku, E. O., Bouillon, S., Tole, M., & Borges, A. V. (2019). Diffusive emissions of methane
546   and nitrous oxide from a cascade of tropical hydropower reservoirs in Kenya. Lakes and
547   Reservoirs: Research and Management, 24(2), 127–135, doi: 10.1111/lre.12264

548   Raymond, P. A., Hartmann, J., Lauerwald, R., Sobek, S., McDonald, C., Hoover, M., et al.
549   (2013). Global carbon dioxide emissions from inland waters. Nature, 503(7476), 355–359,
550   doi: 10.1038/nature12760

551   Read, J. S., Hamilton, D. P., Desai, A. R., Rose, K. C., MacIntyre, S., Lenters, J. D., et al.
552   (2012). Lake-size dependency of wind shear and convection as controls on gas exchange.
553   Geophysical Research Letters, 39(9).

554   Risgaard-Petersen, N. (2003). Coupled nitrification-denitrification in autotrophic and
555   heterotrophic estuarine sediments: On the influence of benthic microalgae. Limnology and
556   Oceanography, 48(1 I), 93–105.

557   Roland, F. A. E., Darchambeau, F., Morana, C., & Borges, A. V. (2017). Nitrous oxide and
558   methane seasonal variability in the epilimnion of a large tropical meromictic lake (Lake
559   Kivu, East-Africa). Aquatic Sciences, 79(2), 209–218, doi: 10.1007/s00027-016-0491-2

560   Seitzinger, S. P., Kroeze, C., & Styles, R. V. (2000). Global distribution of N2O emissions from
561   aquatic systems: Natural emissions and anthropogenic effects. Chemosphere - Global
562   Change Science, 2(3–4), 267–279, doi: 10.1016/S1465-9972(00)00015-5

563   Seitzinger, S. P., Harrison, J. A., Dumont, E., Beusen, A. H. W., & Bouwman, A. F. (2005).
564   Sources and delivery of carbon, nitrogen, and phosphorus to the coastal zone: An overview
565   of Global Nutrient Export from Watersheds (NEWS) models and their application. Global
566   Biogeochemical Cycles, 19(4), doi: Gb4s01 10.1029/2005gb002606

567   Soued, C., del Giorgio, P. A., & Maranger, R. (2015). Nitrous oxide sinks and emissions in
568   boreal aquatic networks in Québec. Nature Geoscience, 9, 116, doi: 10.1038/ngeo2611

569   Thiery, W., Martynov, A., Darchambeau, F., Descy, J.-P., Plisnier, P.-D., Sushama, L., & van
570   Lipzig, N. P. M. (2014). Understanding the performance of the FLake model over two

571 African Great Lakes. Geoscientific Model Development, 7(1), 317–337, doi: 10.5194/gmd-
572 7-317-2014

573 Verpoorter, C., Kutser, T., Seekell, D. A., & Tranvik, L. J. (2014). A global inventory of lakes
574 based on high-resolution satellite imagery. Geophysical Research Letters, 41(18), 6396–
575 6402, doi: 10.1002/2014GL060641

576 Wang, S., Liu, C., Yeager, K. M., Wan, G., Li, J., Tao, F., et al. (2009). agu. Science of the Total
577 Environment, 407(10), 3330–3337, doi: 10.1016/j.scitotenv.2008.10.037

578 Wanninkhof, R. (1992). Relationship Between Wind-Speed and Gas-Exchange Over the Ocean.
579 Journal of Geophysical Research-Oceans, 97(C5), 7373–7382, doi: 10.1029/92jc00188

580 Weiss, R. F., & Price, B. A. (1980). Nitrous oxide solubility in water and seawater. Marine
581 Chemistry, 8(4), 347–359, doi: 10.1016/0304-4203(80)90024-9

582 Whitfield, C. J., Aherne, J., & Baulch, H. M. (2011). Controls on greenhouse gas concentrations
583 in polymictic headwater lakes in Ireland. Science of the Total Environment, 410–411, 217–
584 225, doi: 10.1016/j.scitotenv.2011.09.045

585 Zhu, D., Wu, Y., Wu, N., Chen, H., He, Y., Zhang, Y., et al. (2015). Nitrous oxide emission from
586 infralittoral zone and pelagic zone in a shallow lake: Implications for whole lake flux
587 estimation and lake restoration. Ecological Engineering, 82, 368–375, doi:
588 10.1016/j.ecoleng.2015.05.032

589

590 **Figure 1**: Simulated N$_2$O emissions (N_2O_{em}) as function of water residence time τ_r following
591 scenario DS1 (eq. 7, panel a) and DS2 (eq. 9 panel b). For each scenario, we plotted the function
592 using the EFs of 0.9%, 0.3% and 1.5% (see text). Simulated N_2O_{em} scale linearly with N input
593 from upstream (TN_{in}, DS2) or the sum of TN_{in} and N fixation (*Fix*) (DS1). In this graph, we
594 normalized N_2O_{em} accordingly.

595

596 **Figure 2.** Regional averages of observed vs. simulated N$_2$O emission rates for the two simulation
597 runs DS1 and DS2. The round points correspond to the best model estimates based on an EF=0.9%,
598 the whiskers represent the range defined by alternative lower and upper bound estimates based on
599 *EFs* of 0.3% and 1.5%, respectively. Blue: regions with groups of SWBs; light blue: alternative
600 results for two regions which were constrained by a maximum TN concentration of 26 µM (#5')
601 and 280 µM (#3') as reported in the reference papers (see Table 1); red: single large SWBs. The
602 dashed line represents the 1:1 line. For exact averages and standard deviations in flux rates per
603 region see Table 2.

604

605 **Figure 3.** Simulation results of standing water body (natural lakes and reservoirs) N$_2$O emissions
606 (N_2O_{em}) as a) flux densities per continental area, and b) emission rates per water surface area
607 (N_2O_{em}/A_{water}).

608
609
610

611   **Table 1.** Sources and methodologies used for regionalized, observation based N_2O emission rates
612   used for model evaluation.

613

614   **Table 2.** Regionalized comparison of simulated (best estimate based on EF=0.9%) vs. observation
615   based estimates of N_2O emission rates per water surface area (N_2O_{em}/A_{water}), reported as arithmetic
616   mean rates ±standard deviation. Note that for the Tianjin Region and Ireland, we also report
617   alternative statistics using only SWBs for which the simulated TN concentration do not exceed a
618   threshold value (see text for details).

619

620   **Table 3.** Simulated N_2O emissions per latitudinal zone, continent and type of water body. We
621   report the totals of standing water body area (ΣA_{water}) and N_2O emissions (ΣN_2O_{em}), the
622   contribution of reservoirs to ΣA_{water} and ΣN_2O_{em} (*% reservoirs*), the area weighted mean of N_2O
623   emission rates per water surface area ($\Sigma N_2O_{em}/\Sigma A_{water}$), and the arithmetic means of TN
624   concentrations and water residence time τ_r. Note that for TN concentrations, we calculated the
625   mean from the values between 1st and 99th percentile to avoid the effect of single extreme values.

626

627   **Table 4.** Pearson correlations of model parameters[*]. All parameters have been log-transformed.
628   All reported correlations are statistically significant at a p=0.05 level.

629

630   **Table 5**: Comparison of results with earlier global and zonal estimates of N_2O emissions from
631   natural lakes and reservoirs or from reservoirs only. For each estimate, the total water surface area
632   (ΣA_{water}) and the total N_2O emission flux (ΣN_2O_{em}) are reported. For the upscaling studies cited
633   below, the $\Sigma N_2O_{em}/\Sigma A_{water}$ represents the average observed N_2O emission rate per water surface
634   area which was multiplied by ΣA_{water} to estimate ΣN_2O_{em}. Where ΣN_2O_{em} was estimated based
635   on statistical and process based models (such as in the present study), $\Sigma N_2O_{em}/\Sigma A_{water}$ was
636   calculated for comparison. For studies based on upscaling of observations or statistical models,
637   the number of observations *N* is indicated.

638